Generation of concurrence between two qubits locally coupled to a one-dimensional spin chain

Tanay Nag and Amit Dutta
Department of Physics, Indian Institute of Technology, Kanpur 208 016, India
(Received 25 April 2016; published 15 August 2016)

We consider a generalized central spin model, consisting of two central qubits and an environmental spin chain (with periodic boundary condition) to which these central qubits are locally and weakly connected either at the same site or at two different sites separated by a distance d. Our purpose is to study the subsequent temporal generation of entanglement, quantified by concurrence, when initially the qubits are in an unentangled state. In the equilibrium situation, we show that the concurrence survives for a larger value of d when the environmental spin chain is critical. Importantly, a common feature observed both in the equilibrium and the nonequilibrium situations while the latter is created by a sudden but global change of the environmental transverse field is that the two qubits become maximally entangled for the critical quenching. Following a nonequilibrium evolution of the spin chain, our study for $d \neq 0$ indicates that there exists a threshold time above which concurrence attains a finite value. Additionally, we show that the number of independent decohering channels (DCs) is determined by d as well as the local difference of the transverse field of the two underlying Hamiltonians governing the time evolution; the concurrence can be enhanced by a higher number of independent channels. The qualitatively similar behavior displayed by the concurrence for critical and off-critical quenches, as reported here, is characterized by analyzing the nonequilibrium evolution of these channels. The concurrence is maximum when the decoherence factor or the echo associated with the most rapidly DC decays to zero; on the contrary, the condition when the concurrence vanishes is determined nontrivially by the associated decay of one of the intermediate DCs. Analyzing the reduced density of a single qubit, we also explain the observation that the dephasing rate is always slower than the unentanglement rate. We further establish that the maximally and minimally decohering channels show singular behavior which can be explained by invoking upon a quasiparticle picture.

DOI: 10.1103/PhysRevA.94.022316

I. INTRODUCTION

The notion of entanglement, that emerged from the pioneering work of Einstein, Podolsky, and Rosen [1], is a key concept of quantum computation and quantum information theories [2–5]. Given the recent interest in the studies of quantum correlations in the context of quantum critical systems [6–9], there have been numerous efforts directed to understanding the connection between quantum information and quantum phase transitions (QPTs) [10–16]. Entanglement is usually quantified through two quantum information theoretic measures: (i) concurrence [17–19], a separability based approach to measure the quantum correlation, and (ii) quantum discord [20–22], a measurement based approach for estimating the nonclassical correlations present in a bipartite system. There have also been numerous studies on the entanglement entropy; this is another important tool to probe the entanglement between two blocks of a composite system obtained by measuring the von Neumann entropy associated with the reduced density matrix of one of the blocks [23].

It is now established that the effect of quantum criticality gets imprinted in the behavior of the ground-state correlation which becomes maximum at the quantum critical point (QCP); for example, the concurrence can detect as well as characterize a QPT [10,11]. On the other hand, the entanglement, arising due to the interaction between the system and its environment, leads to decoherence [24]. There exists a plethora of the studies investigating the effects induced by the environment on the quantum information processing [25]; simultaneously, the dynamical control of the decoherence is also being investigated extensively [26,27].

The central spin model (CSM), consisting of a single qubit (spin-1/2) globally coupled to an environmental spin chain, is an important prototypical model to study the Loschmidt echo (LE), also known as the decoherence factor (DF) characterizing the decoherence of the qubit; this has been studied for both equilibrium [28–30] and nonequilibrium [31–39] time evolution and also in the context of dynamical phase transitions [40,41]. Moreover, the concurrence [42] and the quantum discord [43] have been shown to satisfy the universal scaling law as predicted by the Kibble-Zurek argument [44,45] when a parameter of the environmental Hamiltonian is driven linearly across a QCP. Additionally, a generalized central spin model (GCSM) where two spins are globally coupled to an environmental spin chain, with a periodic boundary condition (PBC), is also studied for probing the concurrence and quantum discord generated between the qubits when the composite system evolves in time [46–48]; the concurrence generation is found to be maximum for the critical spin chain [49,50]. In connection to the experimental studies, a QPT has already been observed with ultracold atoms in an optical lattice [51]. A possible realization of a one-dimensional XY chain has also been proposed [52]. Furthermore, using NMR quantum simulator, it has been experimentally confirmed that the LE shows a dip at the QCP of a finite antiferromagnetic Ising spin chain, thereby establishing it an ideal detector of a QCP [53].

Recently, there have been investigations [54,55] of the unentanglement (i.e., the decoherence) between two distant qubits initially entangled and connected to two different sites of the spin chain that evolves in time. The state transfer quality between two external qubits of a spin chain has also been investigated by analyzing the entanglement between them [56]. Given the previous studies, we address the reverse question. Is there a temporal generation of entanglement between a pair

of qubits, initially prepared in an unentangled state, connected at the same site and also two different sites (separated by a distance d) of the environmental spin chain? To address this particular issue, we consider two situations: (i) when the spin chain (chosen to be a one-dimensional transverse Ising chain) evolves temporally in time following the local coupling of the qubits, referred to as the equilibrium situation; (ii) there is an additional sudden global quench of the transverse field of the environmental Hamiltonian in addition to the local coupling, referred to as the nonequilibrium situation. Unlike the above studies, here we investigate the generation of the concurrence in the nonequilibrium situation using a GCSM with a local coupling.

We briefly summarize our main results at the outset: First, we are working in the weak-coupling limit considering a PBC for the environmental spin chain. Our observation for the equilibrium situation is that the entanglement generation is of very small magnitude, although in the vicinity of the QCP of the environment the concurrence becomes maximum and remains small but finite even when the two qubits are separated by a large distance. In the nonequilibrium situation, within the weak-coupling limit, our investigation suggests that the concurrence, of much higher magnitude than the equilibrium case, can be induced by the global and sudden quench of the transverse field; this concurrence eventually decays with time. We explain this generic behavior of the concurrence by analyzing the echoes associated with different decohering channels (DCs) with time; we observe that the number of independent channels is dictated by the separation d and local difference of the transverse field of the two underlying Hamiltonians governing the time evolution. The concurrence attains a higher value for a higher number of independent channels. The decay of the most rapidly decohering channels is responsible for a maximum amount of entanglement while the decay of the concurrence is nontrivially related to the decay of one of the intermediate decaying channels. For a finite separation between the qubits, we establish that the concurrence attains a nonzero value after a threshold time; this is attributed to identical behavior of different DCs up to the threshold time. Additionally, we show that the respective dephasing rate associated with each qubit is always slower than the unentanglement rate between the qubits. Furthermore, we characterize the distance dependent behavior of different DCs following a critical quench by resorting to a quasiparticles picture.

The paper is organized in the following manner. In Sec. II, we introduce the CGCM consisting of two qubits locally connected to two sites of an Ising chain with the transverse field. In parallel, we define the concurrence derived from the 4×4 reduced density matrix of the two qubits obtained by tracing out the environmental degrees of freedom; this density matrix contains different LEs corresponding to different DCs associated with the environmental evolution. In Sec. III the results obtained for the equilibrium situation are presented while in Sec. IV we discuss the nonequilibrium behavior of the concurrence. We analyze the behavior of concurrence observed in equilibrium as well as nonequilibrium cases investigating the temporal evolution of different decohering channels. Finally, we make concluding remarks in Sec. VI.

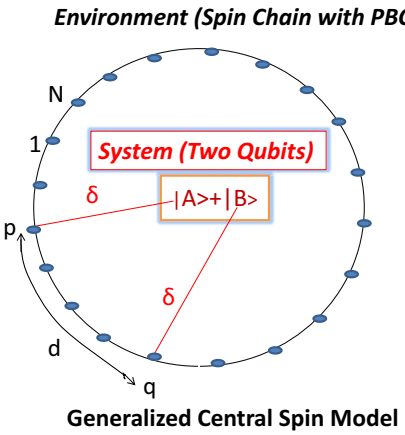

FIG. 1. Schematic diagram shows the generalized central spin model where two qubits A and B are locally connected to two different environmental sites p and q separated from each other by a distance d with a coupling strength δ. We consider a periodic boundary condition for the environmental spin chain with N number of spins.

II. MODEL

We consider a GCSM in which two noninteracting qubits are connected by a local interaction to an environmental spin chain, chosen to be a one-dimensional ferromagnetic (FM) transverse Ising spin model, in such a way that the local transverse field of the environmental spin chain gets modified. The composite system, thus, is a generalization of the central spin model [29], in which a single spin-1/2 particle (qubit) is globally connected to all the spins of the environmental spin chain with an interaction Hamiltonian; the schematic diagram of the GCSM is shown in Fig. 1. The combined Hamiltonian H_{T}, comprising an environmental transverse Ising Hamiltonian H_{E} [9] with N number of spins and interaction Hamiltonian H_{SE} of two qubits, is given by

$$H_T = H_{SE} + H_E. \tag{1}$$

Here,

$$H_E = -J \sum_n \sigma_n^x \sigma_{n+1}^x - \lambda \sum_n \sigma_n^z, \tag{2}$$

where σ's are the usual Pauli matrices. λ and J (set equal to unity below) are the transverse magnetic field and ferromagnetic cooperative interactions, respectively. We consider a PBC $\sigma_{N+1}^i = \sigma_1^i$. The interaction Hamiltonian for two qubits A and B connected at different sites of the environment is given by

$$H_{SE} = -\delta\left(|\uparrow\rangle\langle\uparrow|_A \otimes \sigma_p^z + |\uparrow\rangle\langle\uparrow|_B \otimes \sigma_q^z\right); \tag{3}$$

here, $|\uparrow\rangle_{A,B}$ is an eigenstate of $\sigma_{A,B}^z$ satisfying $\sigma_{A,B}^z|\uparrow\rangle_{A,B} = |\uparrow\rangle_{A,B}$, while $\sigma_{p,q}^z$ denote the environmental spin at pth and qth site, respectively; these sites are separated by a distance d. δ is the coupling strength and we shall work in the limit $\delta \ll 1$, which we shall address as the weak-coupling limit. Clearly, the interaction Hamiltonian (3) suggests that interaction with the qubits modifies the local transverse field of the environment.

In order to study the generation of concurrence between two qubits, we take a completely unentangled (direct product)

initial state given by

$$|\phi\rangle_{AB} = \tfrac{1}{2}(|\uparrow\rangle_A + |\downarrow\rangle_A) \otimes (|\uparrow\rangle_B + |\downarrow\rangle_B). \tag{4}$$

The initial state for the composite system is then given by $|\psi(\lambda_i,t=0)\rangle = |\phi\rangle_{AB} \otimes |\eta(\lambda_i,t=0)\rangle$, where $|\eta(\lambda_i,t=0)\rangle$ is the initial ground state of the environmental Hamiltonian H_E given in Eq. (2).

Focusing on the nonequilibrium situation, we consider a sudden quenching of the transverse field which is instantaneously changed from an initial value λ_i to a final value λ_f and study the subsequent temporal evolution of the composite system. We note that the equilibrium situation corresponds to $\lambda_f = \lambda_i$. Depending upon the state of the qubits, the interaction Hamiltonian leads to four channels of evolution for the environment. The channel Hamiltonians $H_{\alpha\beta}$ with λ_f governing the dynamics are given by

$$\begin{aligned} H_{\downarrow\downarrow}(\lambda_f) &= H_E(\lambda_f), \\ H_{\uparrow\uparrow}(\lambda_f) &= H_E(\lambda_f) - \delta\big(\sigma_p^z + \sigma_q^z\big), \\ H_{\downarrow\uparrow}(\lambda_f) &= H_E(\lambda_f) - \delta\sigma_q^z, \\ H_{\uparrow\downarrow}(\lambda_f) &= H_E(\lambda_f) - \delta\sigma_p^z. \end{aligned} \tag{5}$$

The time evolved state of the composite system is given by

$$\begin{aligned} |\psi(t)\rangle = \tfrac{1}{2}(&|\uparrow\uparrow\rangle \otimes |\eta_{\uparrow\uparrow}(t)\rangle + |\downarrow\downarrow\rangle \otimes |\eta_{\downarrow\downarrow}(t)\rangle \\ &+ |\uparrow\downarrow\rangle \otimes |\eta_{\uparrow\downarrow}(t)\rangle + |\downarrow\uparrow\rangle \otimes |\eta_{\downarrow\uparrow}(t)\rangle), \end{aligned} \tag{6}$$

where $|\alpha\beta\rangle$ represents the state for two qubits and environmental evolved state $|\eta_{\alpha\beta}(t)\rangle$ is given by

$$|\eta_{\alpha\beta}(t)\rangle = e^{-iH_{\alpha\beta}t}|\eta(\lambda_i,t=0)\rangle, \tag{7}$$

where λ_i is the initial homogeneous transverse field same for all sites, i.e., $\lambda_n = \lambda_i$.

One can construct the reduced density matrix of the qubits by tracing out the environmental degrees of freedom from the composite density matrix constructed from $|\psi(t)\rangle$. The reduced density matrix for the two qubits system in the basis $\{|\uparrow\uparrow\rangle,|\uparrow\downarrow\rangle,|\downarrow\uparrow\rangle,|\downarrow\downarrow\rangle\}$ is given by

$$\rho_s(t) = \frac{1}{4}\begin{bmatrix} 1 & d_{\uparrow\uparrow,\uparrow\downarrow} & d_{\uparrow\uparrow,\downarrow\uparrow} & d_{\uparrow\uparrow,\downarrow\downarrow} \\ d^*_{\uparrow\uparrow,\uparrow\downarrow} & 1 & d_{\uparrow\downarrow,\downarrow\uparrow} & d_{\uparrow\downarrow,\downarrow\downarrow} \\ d^*_{\uparrow\uparrow,\downarrow\uparrow} & d^*_{\uparrow\downarrow,\downarrow\uparrow} & 1 & d_{\downarrow\uparrow,\downarrow\downarrow} \\ d^*_{\uparrow\uparrow,\downarrow\downarrow} & d^*_{\uparrow\downarrow,\downarrow\downarrow} & d^*_{\downarrow\uparrow,\downarrow\downarrow} & 1 \end{bmatrix}, \tag{8}$$

where $d_{\alpha\beta,\gamma\lambda} = \langle\eta_{\alpha\beta}(t)|\eta_{\gamma\lambda}(t)\rangle$, with $\alpha,\beta,\gamma,\lambda$ are binary variables representing $\uparrow$ and $\downarrow$. The LEs corresponding to different channels are $D_{\alpha\beta,\gamma\lambda}(t) = |d_{\alpha\beta,\gamma\lambda}(t)|^2$ and its explicit form is the following:

$$D_{\alpha\beta,\gamma\lambda}(t) = |\langle\eta(\lambda_i)|e^{iH_{\alpha\beta}(\lambda_f)t}e^{-iH_{\gamma\lambda}(\lambda_f)t}|\eta(\lambda_i)\rangle|^2. \tag{9}$$

Now, using the density matrix $\rho_s(t)$ given in Eq. (8), one can compute the concurrence between the two qubits. We shall follow Wooter's definition of concurrence given by

$$C(\rho_s) = \max(0,\sqrt{\epsilon_1} - \sqrt{\epsilon_2} - \sqrt{\epsilon_3} - \sqrt{\epsilon_4}), \tag{10}$$

where ϵ_i's are the eigenvalues in a descending order of the non-Hermitian matrix $M = \rho_s\hat{\rho}_s$ with $\hat{\rho}_s$ defined as

$$\hat{\rho}_s = (\sigma^y \otimes \sigma^y)\rho_s^*(\sigma^y \otimes \sigma^y). \tag{11}$$

Therefore, one readily concludes that the concurrence between the two qubits are determined by the LE associated with the four channels. It is to be noted that the concurrence and LEs are all dimensionless numbers and bounded between 0 and 1; also, time is measured in appropriate dimension setting $\hbar = 1$. In this paper, we consider all the logarithms to the base e.

Let us consider a generic Hamiltonian of a one-dimensional Ising chain in a site dependent transverse field λ_n given by

$$H = -\sum_n \big(\sigma_n^x\sigma_{n+1}^x + \lambda_n\sigma_n^z\big). \tag{12}$$

One can obtain the initial Hamiltonian from the above Hamiltonian (12) by setting $\lambda_n = \lambda$ while for the final Hamiltonian λ_n becomes different from λ at those sites where the qubits are coupled. For the initial homogeneous case ($\lambda_n = \lambda$), the model in Eq. (12) has a QCP at $J = \lambda$ separating FM and quantum paramagnetic (PM) phases. Using Jordan-Wigner transformations followed by Fourier transformation for a homogeneous and periodic chain, the energy spectrum for the Hamiltonian in Eq. (12) is obtained as [57,58]

$$\varepsilon_q = \pm 2\sqrt{(\lambda + \cos q)^2 + \sin^2 q}, \tag{13}$$

where q is the momentum which takes discrete values given by $q = 2\pi m/N$ with $m = 0,\ldots,N-1$ for a finite system of length N.

In order to express the LE given in Eq. (9) in the fermionic representation one has to cast the Hamiltonian in the above basis following Jordan-Wigner transformation. The Hamiltonian in Eq. (12) can be described by a quadratic form in terms of spinless fermions c_i and $c_i^\dagger$ [57,58],

$$H = \sum_{i,j}\big[c_i^\dagger A_{i,j}c_j + \tfrac{1}{2}(c_i^\dagger B_{i,j}c_j^\dagger + \text{H.c.})\big]. \tag{14}$$

Here, A is a symmetric matrix as H is Hermitian and B is an antisymmetric matrix which follows from the anticommutation rules of c_i's. The elements of these matrices thus obtained are

$$\begin{aligned} A_{i,j} &= -(J\delta_{j,i+1} + J\delta_{i,j+1}) - 2\lambda_j\delta_{i,j}, \\ B_{i,j} &= -(J\delta_{j,i+1} - J\delta_{i,j+1}), \end{aligned} \tag{15}$$

where λ_j is the site dependent transverse field.

The Hamiltonian (14) can be written in the following form also:

$$H = \tfrac{1}{2}\Psi^\dagger\mathcal{H}\Psi, \tag{16}$$

with $\Psi = (c^\dagger,c) = (c_1^\dagger,\ldots,c_N^\dagger,c_1,\ldots,c_N)$ and $\mathcal{H}$ is given by

$$\mathcal{H} = \begin{bmatrix} -A & -B \\ B & A \end{bmatrix}. \tag{17}$$

The above Hamiltonian can be diagonalized in terms of the normal-mode spinless Fermi operators η_k given by the relation [57]

$$\eta_k = \sum_i [g_k(i)c_i + h_k(i)c_i^\dagger], \tag{18}$$

where $g_k(i)$ and $h_k(i)$ are real numbers; $g_k(i)$ and $h_k(i)$ are obtained from the real matrices g and h, respectively.

The unitary matrix U that diagonalizes the Hamiltonian given in Eq. (17) can be constructed from $g_k(i)$ and $h_k(i)$,

$$U = \begin{bmatrix} g & h \\ h & g \end{bmatrix}. \tag{19}$$

Using this unitary operator one can also write the fermionic operator in terms of normal modes,

$$c_i = \sum_k [g_k(i)\eta_k + h_k(i)\eta_k^\dagger]. \tag{20}$$

In terms of the new operators η_k, the Hamiltonian in Eq. (17) takes the diagonal form,

$$H = \sum_k \Lambda_k \left(\eta_k^\dagger \eta_k - \frac{1}{2}\right), \tag{21}$$

with Λ_k being the energy of different fermionic modes with index k.

In order to study the time evolution of concurrence C, we have to first compute the time-dependent LE that constitutes the reduced density matrix of two spins given in Eq. (8). One can use the covariance matrix formalism to determine time evolution of LE associated with the different DCs governed by two different Hamiltonians [55,59]. These different Hamiltonians $H_{\alpha\beta}$ shown in Eq. (5) have different sets of local transverse fields. This formalism allows us to write the LE in the following way:

$$D_{\alpha\beta,\gamma\lambda}(t) = |\det[I - R_{\alpha\beta}(t) - R_{\gamma\lambda}(t)]|^{1/2}. \tag{22}$$

Here, I is an identity matrix and $R_{\alpha\beta}(t)$'s are the time evolved covariant matrices given by

$$R_{\alpha\beta}(t) = e^{-iH_{\alpha\beta}t} R(0) e^{iH_{\alpha\beta}t} \tag{23}$$

with $R(0) = \langle \eta(\lambda_i, t=0) | \Psi\Psi^\dagger | \eta(\lambda_i, t=0) \rangle$, and its matrix form is given by

$$R(0) = \begin{bmatrix} \langle c^\dagger c \rangle & \langle c^\dagger c^\dagger \rangle \\ \langle cc \rangle & \langle cc^\dagger \rangle \end{bmatrix} = \begin{bmatrix} h^T h & h^T g \\ g^T h & g^T g \end{bmatrix}, \tag{24}$$

where T denotes the transpose of a matrix. This $2N \times 2N$ initial covariant matrix is composed of four blocks and all of these blocks are having the same dimension of $N \times N$.

III. EQUILIBRIUM STUDY

In this section, we shall illustrate the equilibrium behavior of concurrence given in Eq. (10) as a function of time when the environment evolves along different DCs originated from the coupling to the qubit. In this case $\lambda_i = \lambda_f = \lambda$, for all the sites except the sites where the qubits are locally connected. Figure 2(a) depicts the behavior of concurrence for $d = 0$ while Fig. 2(b) shows it for $d = 1$. When the parameter value is chosen to be close to the quantum critical value ($\lambda = 0.99$), the concurrence initially grows as a function of time showing a prominent dip at $t = N/v = N/2$ and subsequent revival; this is because of the constructive interference of quasiparticles generated due to the local connection of the qubit to the spin chain having group velocity $v = 2$ at the QCP. Thus, the finite-size effect is manifested in this dip of the LE which is prominent for $\lambda = 1$. In the PM phase also, concurrence shows

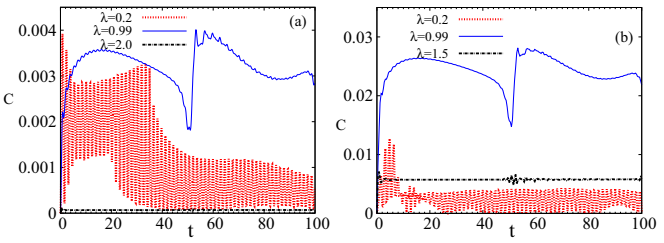

FIG. 2. Plot (a) shows the equilibrium behavior of concurrence C as a function of time with both the qubits connected at the same site, i.e., $d = 0$, for different phases (FM and PM phase) including the QCP of the environmental chain; plot (b) shows the variation of C as a function of time when $d = 1$. In both cases, the generation of entanglement is of small magnitude. We consider $N = 100$ and $\delta = 0.1$.

rapid fluctuations of small amplitude at around $t = N/2$; otherwise, it shows a time-independent behavior. Comparing Fig. 2(a) with Fig. 2(b), one can see that C is one order of magnitude greater for $d = 1$ than for the $d = 0$ case. As we shall discuss in Sec. V in the context of Fig. 7, for the case $d = 1$, there are additional independent channels with different LEs [see Eq. (9)] resulting in more prominent interference effects; however, in the nonequlibrium case (see Fig. 5) there exits additional channels for $d = 0$ also. What is noteworthy is that even if the qubits are initially unentangled, there is a generation concurrence only due to the local coupling during the temporal evolution of the composite system.

Additionally, maximum concurrence is generated when λ is close to the critical value (when there is a diverging length scale) rather than in the PM and FM phases. That the value of the concurrence attains maximum for $\lambda \simeq 1$ is independent of the distance d between the qubits and hence is a universal observation. We however note that in the weak-coupling limit the magnitude of the maximum value of the concurrence thus generated is smaller in contrast to the nonequilibrium case to be discussed in the next section, although, it should be noted that in the relatively strong-coupling limit the maximum value of concurrence (see Fig. 3) in the equilibrium case is of the

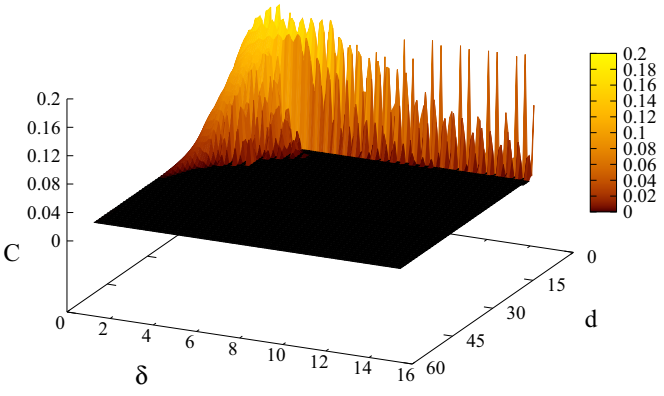

FIG. 3. Plot shows the variation of C as a function of distance d (with $d > 0$) and coupling strength δ when $\lambda = 0.99$ (QCP), $N = 100$, and $t = 7.3$. In the weak-coupling limit the concurrence is nonzero for relatively larger separation d.

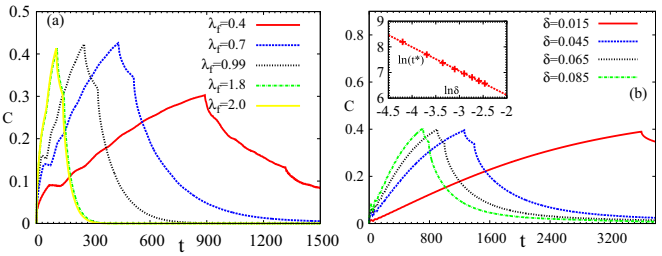

FIG. 4. Plot (a) shows the variation of C as a function of time followed by a sudden quench of the transverse field of the environmental Ising chain choosing the environment initially in the FM phase. The concurrence initially increases and eventually decays to zero showing a primary peak at $t = t^*$ and a secondary peak at $t = t_2 > t^*$; t^* and t_2 both decrease with the quench amplitude $|\lambda_i - \lambda_f|$. Here, $\lambda_i = 0.2$ and $\delta = 0.1$. Plot (b) shows the variation of C as a function of time when the spin chain is quenched from the PM phase with $\lambda_i = 1.5$ to QCP at $\lambda_f = 0.99$ for different values of δ. Inset shows the variation of t^* with δ within the weak-coupling limit, $t^* \propto \delta^{-1}$. Here, it has been shown that $\ln(t^*)$ is linearly proportional to $\ln(\delta)$ with a slope $\simeq -0.93$; the logarithm is to the base e. For both the above cases, we consider $d = 0$ and $N = 100$.

same order of magnitude as the nonequilibrium case shown in Figs. 4 and 5 for small δ limit.

A close inspection of Fig. 3 suggests that for the strong-coupling limit with $\delta > 1$, the concurrence becomes finite for only short distance $1 < d < 3$. In contrary, the concurrence gradually decreases over a relatively large distance (starting from $d = 1$) in the weak-coupling limit $\delta < 1$, although the magnitude of C is small compared to the $\delta > 1$ regime. For relatively strong-coupling strength $\delta \sim O(1)$, the concurrence becomes maximum (reaching a value around 0.19) for small d.

A large value of $\delta(\gg 1)$ makes the value of the local transverse field off-critical so that the correlation become short ranged and consequently the entanglement between two distant qubits is vanishingly small while for small $\delta(\ll 1)$ the

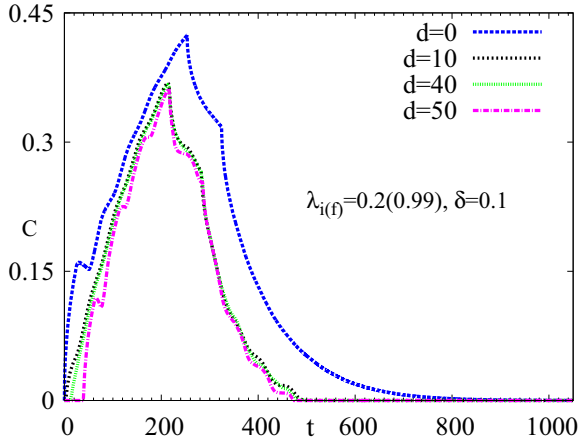

FIG. 5. Figure shows the variation of C as a function of time with distance d as the parameter when the environmental chain is quenched from the FM phase to QCP. The concurrence becomes maximum for $d = 0$; there exists a threshold time $t_{\rm TH}$ above which C attains a finite value for $d \neq 0$.

value of the local transverse field stays critical and hence a long-range correlation exists in the environment. There exists a pronounced oscillatory behavior of C as a function of δ for two qubits coupled within a small distance d between them. This is explained noting that the concurrence is derived from $D_{\alpha,\beta,\gamma,\lambda}$ having sinusoidal factors like $\cos^2[E_{\alpha\beta}(\delta)t]$ where $E_{\alpha\beta}(\delta)$ is the eigenvalues of the Hamiltonian $H_{\alpha\beta}(\delta)$ [Eq. (5)]. Therefore, when t and d are kept fixed, different LEs [see Eq. (9)] exhibit oscillating behavior with δ which then gets reflected into concurrence. However, we are interested in the weak-coupling limit, hence these oscillations are not going to influence the results presented in the subsequent discussions.

IV. NONEQUILIBRIUM STUDY

We shall now extend the previous studies to the situation in which the environmental spin chain undergoes a global sudden quenching, i.e., the transverse field λ is suddenly changed from an initial value λ_i to a final value λ_f. In this nonequilibrium situation, two external qubits become more strongly entangled as compared to the earlier equilibrium situation. Results presented in Fig. 4(a) suggest the following: (i) The concurrence generation is maximum when the spin chain is quenched to the QCP starting from the FM phase. (ii) Quenching within the same phase yields entanglement of smaller magnitude between the qubits as compared to the quenching between two different phases. Furthermore, concurrence remains nonzero for longer time if the quenching is performed within the same phase. Finally, there is a prominent peak in C appearing at time $t = t^*$ that becomes smaller for higher quench amplitude. Additionally, there exists a secondary peak at $t = t_2$ after the primary peak at t^*. On the other hand, we show in Fig. 4(b) that t^* decreases with δ, in fact, is inversely proportional to δ as shown in the inset. We note that the above features of C is qualitatively identical for all types of quenching protocols. Comparing the results presented in Figs. 3 and Fig. 4, we can infer that the large δ equilibrium case is equivalent to the small δ nonequilibrium case so far as the concurrence generation is concerned.

Figure 5 shows that for the critical quenching starting from the FM phase, C becomes maximum for $d = 0$ while for other cases with $d \neq 0$, it attains a finite value only after a threshold time $t_{\rm TH}$; this threshold time increases with the increasing d. One can note that t^* attains a higher value for $d = 0$ as compared to the case $d \neq 0$; in the latter case, t^* almost remains constant. Additionally, we observe that C stays at a nonzero value for longer time for $d = 0$ as compared to $d \neq 0$ case. The maximization of C for $d = 0$ case may be related to the relatively strong interference between a larger number of independent LEs as compared to the finite d case where two of the LEs behave identically. We shall elaborate it further in Sec. V while discussing Figs. 9 and 10. The interference effect is also hinted in Figs. 2(a) and 2(b) for the equilibrium case.

V. INTERPRETATION USING CHANNEL ANALYSIS

In this section, we shall analyze the results presented in previous sections using the LEs associated with the different DCs which in turn lead to the generation of entanglement between the qubits which are initially unentangled. For this

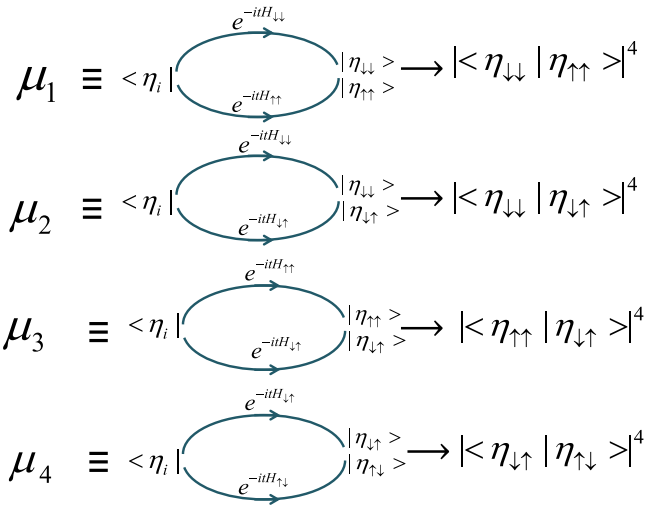

FIG. 6. Schematic diagram explicitly shows the formation of four channels μ_1, μ_2, μ_3, and μ_4 with their underlying Hamiltonians $H_{\alpha\beta}$; μ_1 is governed by $H_{\uparrow\uparrow}$ and $H_{\downarrow\downarrow}$, μ_2 by $H_{\downarrow\downarrow}$ and $H_{\downarrow\uparrow}$, μ_3 by $H_{\uparrow\uparrow}$ and $H_{\downarrow\uparrow}$, and μ_4 by $H_{\downarrow\uparrow}$ and $H_{\uparrow\downarrow}$.

purpose, let us fix our notation first: $D^2_{\alpha\beta,\gamma\lambda} = |\det(I - R_{\alpha\beta} - R_{\gamma\lambda})| = |d_{\alpha\beta,\lambda\gamma}|^4$. Recalling Eq. (9), we have $D^2_{\downarrow\downarrow,\uparrow\uparrow} = \mu_1$; periodic boundary condition ensures that $D^2_{\downarrow\downarrow,\uparrow\downarrow} = D^2_{\downarrow\downarrow,\downarrow\uparrow} = \mu_2$, $D^2_{\uparrow\uparrow,\uparrow\downarrow} = D^2_{\uparrow\uparrow,\downarrow\uparrow} = \mu_3$ (hence, this is valid for all d as well as for equilibrium and nonequilibrium cases) and $D^2_{\downarrow\uparrow,\uparrow\downarrow} = \mu_4$. We therefore have to deal with these four DCs to analyze the temporal behavior of C. We shall refer to μ_1, μ_2, μ_3, and μ_4 as DCs in the subsequent discussion and figures.

We reiterate that there are total of four governing Hamiltonians $H_{\alpha\beta}$ (with $\alpha,\beta = \uparrow,\downarrow$) as given in Eq. (5) depending on the spatial configuration of the local coupling term [see Eq. (3)]. These Hamiltonians ultimately dictate the behavior of C through the DCs i.e., μ_1, μ_2, μ_3, and μ_4. One can see that $H_{\uparrow\uparrow}$ is the maximally deviated from the unperturbed Hamiltonian $H_{\downarrow\downarrow}$ and other two Hamiltonians $H_{\uparrow\downarrow}$ and $H_{\downarrow\uparrow}$ are deviated from $H_{\downarrow\downarrow}$ by just one local transverse field term. The schematic diagram as shown in Fig. 6 depicts these different Hamiltonians $H_{\uparrow\uparrow}$, $H_{\uparrow\downarrow}$, $H_{\downarrow\uparrow}$, and $H_{\downarrow\downarrow}$ that govern the time evolution of four DCs. We note that μ_2 and μ_3 may behave in an identical fashion; moreover, for the $d = 0$ case, μ_4 trivially becomes unity throughout whereas μ_1, μ_2, and μ_3 never become unity. For $d \neq 0$, none of these μ_n's becomes unity. We shall investigate each of these DCs in subsequent discussions at length.

Let us first investigate the behavior of individual channel in the equilibrium scenario. In a generic situation all the DCs are independent with their corresponding LEs $\sqrt[4]{\mu_1}$, $\sqrt[4]{\mu_2}$, $\sqrt[4]{\mu_3}$, and $\sqrt[4]{\mu_4}$. Figure 7(a) represents the temporal behavior of different DCs for $d = 0$ when the environment is in the FM phase. The channel μ_4 does not have a dynamics and hence remains trivially unity for all time due to the fact that the initial state evolves with two identical Hamiltonians, both with an additional transverse field δ at one site. In the weak-coupling limit $\delta \to 0$, $\mu_2 \simeq \mu_3$; therefore, one can approximately work with two independent DCs, μ_1 and μ_2. This can be attributed to the fact that the underlying Hamiltonians are different from

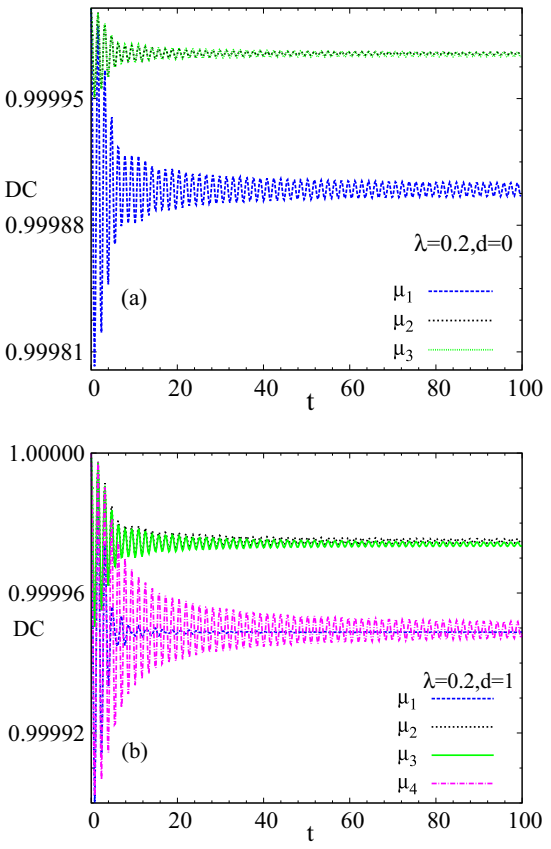

FIG. 7. Equilibrium echo for different DCs μ_1, μ_2, and μ_3 as a function of time are plotted when the spin chain is in the FM phase. Plot (a) represents $d = 0$ case while the plot (b) depicts the behavior of DCs along with an additional channel μ_4 for $d = 1$ case. We observe that μ_3 superimposes on μ_2 leading to two nontrivial independent channels for $d = 0$ case as explained in the text. On the other hand, for finite distance between the qubits, μ_2 deviates from μ_3 which is more prominent in late time region. In addition, there is an extra independent channel μ_4 which is no longer trivially unity like the earlier $d = 0$ case. For both cases we consider, $N = 100$, $\delta = 0.01$.

each other in an identical way, i.e., at a single coupling site only the local transverse field of one of the Hamiltonians is deviated by δ from the other. These observations lead us to the conclusion that for $d = 0$ and within the weak-coupling limit, the number of independent channels effectively depends on the corresponding difference in the local fields of two underlying Hamiltonians that dictate the time evolution of the initial state; the differences in this case are δ for μ_2 and 2δ for μ_1.

Figure 7(b) represents the temporal behavior of different DCs for $d = 1$ when the environment is in the FM phase. Interestingly, μ_4 in this case is not trivially unity as in the previous case of $d = 0$. In this case for $d \neq 0$ and $\delta \ll 1$, where indeed we have four independent channels though for $\delta \to 0$, there is a significant overlap between μ_2 and μ_3; however, μ_2 deviates from μ_3 which is more prominent in the large time limit, as δ increases. This deviation may be originated from the fluctuations coming from the local details of the underlying Hamiltonians associated with the transverse field at two different coupling sites, i.e., $H_{\downarrow\downarrow}$, $H_{\downarrow\uparrow}$ for μ_2 and $H_{\uparrow\uparrow}$, $H_{\downarrow\uparrow}$ for μ_3, and that is why this deviation is eminent in

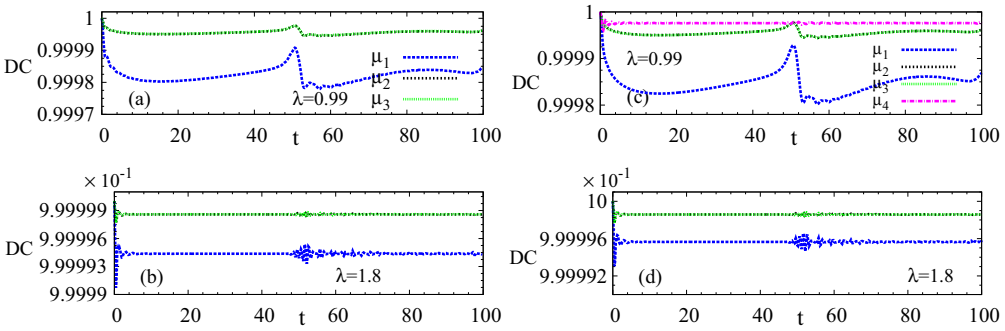

FIG. 8. The temporal behavior of equilibrium echo for different DCs are plotted when the spin chain is at the QCP with $d = 0$ (a), $d = 1$ (c), and in the PM phase with $d = 0$ (b), $d = 1$ (d). The DCs in PM phase deviate minimally from the initial value, i.e., unity, and behave almost independent of time except around $t = N/v = 50$ where DCs exhibit rapid fluctuations. On the other hand, decoherence effect is stronger resulting in a noticeable temporal variation of these DCs. For both the cases we consider, $N = 100$, $\delta = 0.01$.

Fig. 7(b) as compared to Fig. 7(a). In this FM phase, μ_1 and μ_4 almost overlap with each other; μ_1 in the above phase shows prominent oscillations as one increases d.

Figures 8(a) and 8(b) represent the temporal behavior of different DCs for $d = 0$ when the environment is at QCP and in the PM phase, respectively, while Figs. 8(c) and 8(d) correspond to the $d = 1$ case. Comparing Figs. 7(a) and 8(a) and 8(b), the other notable point is that μ_2, calculated in different phases and at QCP, always remains at a higher value than that of μ_1. This can be attributed to the fact that μ_1 exhibits a sharper short time fall than that of μ_2. Comparing Figs. 7(b) and 8(c) and 8(d), one can see that in the FM phase μ_2 is always higher than μ_1 and μ_4. On the other hand, in the PM phase or at the QCP $\mu_4 > \mu_2 > \mu_1$. One can hence conclude that for $d \neq 0$ the channel μ_4 is maximally affected in the FM phase as compared to the QCP and PM phases. In all the cases discussed above, μ_1 is maximally deviated from unity during its temporal evolution.

We shall now compare the dephasing rate of a single qubit [60] with the temporal decay of the concurrence which is generated following a nonequilibrium evolution. This is calculated invoking upon the reduced 2×2 density matrix $\rho_{A(B)}$ of the qubit $A(B)$ that is obtained by tracing over one of the qubits from the 4×4 density matrix of the two-qubit system as in (8). Here, the off-diagonal terms of the reduced density matrix are called the dephasing factor (DP); these terms are denoted by $S_{A(B)}(t)$ to quantify the loss of coherence of a single qubit which was initially prepared in a pure state with another qubit. The decay of $S_{A(B)}(t)$ as a function of time, therefore, determines the time over which the coherence vanishes. Tracing over one of the qubits in Eq. (8), one gets

$$\rho_A(t) = \rho_B(t) = \frac{1}{2}\begin{bmatrix} 1 & \frac{\sqrt{\mu_3'}+\sqrt{\mu_2'}}{2} \\ \frac{\sqrt{\mu_3'}+\sqrt{\mu_2'}}{2} & 1 \end{bmatrix}, \qquad (25)$$

where $\mu_n' = \sqrt{\mu_n}$. Remarkably, the off-diagonal terms $S_{\rm A}(t) = S_{\rm B}(t) = (\sqrt{\mu_3'} + \sqrt{\mu_2'})/4$ are completely independent of μ_1 and μ_4; this leads to an interesting consequence as we shall elaborate below.

Now, we focus on the nonequilibrium evolution of the channel choosing $d = 0$ first. Here, one has four independent channels unless $\delta \to 0$ when μ_2 coincides with μ_3 though μ_4 becomes trivially identity as in the equilibrium case. Figures 9(a)–9(c) show nonequilibrium temporal evolution of C, DC, and DP with $d = 0$ for the FM, the critical, and the PM quenching while the initial state of the environment is in the FM phase, respectively. One can see that the primary peak of the concurrence occurs when $\mu_1 \to 0$ and the secondary peak when $\mu_2\mu_3 \to 0$. To be more precise, the secondary peak appears when $\mu_3 \to 0$ but μ_2 is finite and hence their product $\mu_2\mu_3 \to 0$. On the other hand, concurrence becomes vanishingly small when $\mu_3^{1/2} \to 0$. Additionally, one can see that in the early time region μ_2 almost overlaps with μ_3 but in the course of the evolution, these two channels start to behave differently leading to a visible deviation from each other. Recalling $S_{A(B)}$ we find that there exists a finite coherence even long after the qubits become unentangled from each other; this implies that the dephasing rate is slower than the rate in which the qubits lose the entanglement [60]. This observation is qualitatively explained as follows: the DCs μ_2 and μ_3 appear in the DP S_A and S_B in an additive manner; on the other

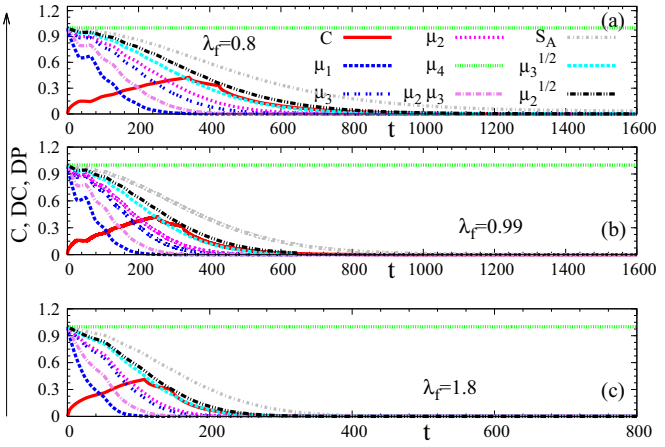

FIG. 9. Nonequilibrium echos for different DCs, DP, and C are plotted as a function of time with three different situations: quenching to the FM phase with $\lambda_f = 0.8$ (a), quenching to the QCP with $\lambda_f = 0.99$ (b), and quenching to the PM phase where $\lambda_f = 1.8$ (c). Here, $N = 100$, $\delta = 0.1$, $d = 0$, and $\lambda_i = 0.2$. μ_1 displays the sharpest decay to zero among all the four channels. μ_4 exhibits time-independent behavior and μ_3 vanishes more rapidly than μ_2.

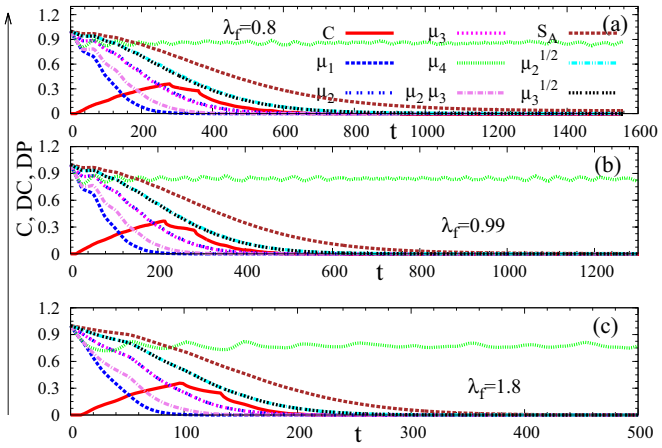

FIG. 10. DC, DP, and C for $d = 40$ are plotted as a function of time with three different situations, quenching to the FM phase with $\lambda_f = 0.8$ (a), quenching to QCP with $\lambda_f = 0.99$ (b), quenching to the PM phase where $\lambda_f = 1.8$ (c). Here, $N = 100$, $\delta = 0.1$, and $\lambda_i = 0.2$. There exists a threshold time $t_{\rm TH}$ above which C attains a nonzero value. The dynamical behavior of μ_2 coincides with that of the μ_3 throughout the temporal evolution.

hand, concurrence depends on the μ's in a complicated way. We therefore observe a long dephasing time $T_{\rm D}$ (dictating the decay of S_A and S_B) as compared to unentanglement time $t_{\rm UE}$ above which the concurrence vanishes between the two qubits. Additionally, $T_{\rm D} \gg T_{\rm UE}$ for FM quenching whereas $T_{\rm D}$ is comparable (of the same order) to $T_{\rm UE}$ for the PM quenching case and the quantum critical case. All the above observations are independent of the quenching path i.e., sudden quenching within the same phase or to QCP or to a different phase.

In parallel, Figs. 10(a)–10(c) represent the time evolution of C, DC, and DP with $d = 40$ for the FM, critical, and the PM quenching, and the initial state in the FM phase, respectively. For this $d \neq 0$ case, the μ_4 exhibits improper oscillations with time. μ_4 remains the minimally affected channel in the nonequilibrium situations like the equilibrium situations as it always lies close to unity. But the main difference with the $d = 0$ case is that μ_3 and μ_2 almost always coincide with each other even when δ is not vanishingly small. Therefore, here we have three independent channels μ_1, μ_2, and μ_4. It shows that the primary peak of C occurs when $\mu_1 \to 0$ and the secondary peak is obtained when $\mu_2\mu_3 \simeq \mu_2^2 \to 0$. A detailed observation suggests that μ_2 and μ_3 both become sufficiently small ($\sim$0.15); as a result their product $\mu_2\mu_3 \to 0$. The concurrence becomes vanishingly small when $\mu_3 \to 0$. In all the phases $\mu_2^{1/2}$ and $\mu_3^{1/2}$ remain finite even after concurrence vanishes. The other notable feature of this finite d case is that the $T_{UE} \simeq T_D/2$ for critical and PM quenching. $T_D \gg T_{UE}$ for the FM quenching case which has also been observed for the $d = 0$ situation. One remarkable observation for $d \neq 0$ is that up to a threshold time $t_{\rm TH}$, concurrence remains zero and different DCs overlap with each other; for $t < t_{\rm TH}$, we see that $\mu_4 \simeq \mu_1$ and $\mu_3^2 \simeq \mu_1$ and after this threshold time the different DCs move away from each other except for the channels μ_2 and μ_3. We observe that C can only take a positive value after $t_{\rm TH}$ as shown in Fig. 5.

Comparing the results presented in Figs. 9 and 10, we note that for $d = 0$, $H_{\downarrow\uparrow}$ determining the evolution of μ_2 has a local transverse field modified by only δ with respect to the final unperturbed Hamiltonian $H_{\downarrow\downarrow}$ in which there is an effect of coupling; on the other hand, $H_{\uparrow\uparrow}$ in μ_3 has a local field modified by 2δ. Hence, μ_2 and μ_3 behave differently with time. One can infer that the dynamical evolution of μ_2 matches with that of the μ_3 only in the $\delta \to 0$ limit as we have already mentioned earlier. Now, for $d \neq 0$, the underlying Hamiltonians $H_{\downarrow\uparrow}$, $H_{\uparrow\uparrow}$ governing the dynamics of μ_2 and μ_3 are similar in the sense that both of them are having the identically modified transverse fields by just an amount δ at two different sites over the Hamiltonian $H_{\downarrow\downarrow}$. This explains the observation that the temporal evolution μ_2 and μ_3 are identical and they fall on top of each other with time. In a nutshell, our study suggests that the square of the LEs (μ_n's) themselves are more important than the LEs ($\sqrt{\mu_n}$'s) in determining the behavior of the concurrence, although its decay may depend on the LEs. The conditions of appearance of the first and second peak of C are universal for any d.

One can write the composite density matrix of two qubits in a generic form, valid for equilibrium as well as nonequilibrium situations, given by

$$\rho_s(t) = \frac{1}{4}\begin{bmatrix} 1 & \sqrt{\mu_3'} & \sqrt{\mu_3'} & \sqrt{\mu_1'} \\ \sqrt{\mu_3'} & 1 & \sqrt{\mu_4'} & \sqrt{\mu_2'} \\ \sqrt{\mu_3'} & \sqrt{\mu_4'} & 1 & \sqrt{\mu_2'} \\ \sqrt{\mu_1'} & \sqrt{\mu_2'} & \sqrt{\mu_2'} & 1 \end{bmatrix}. \tag{26}$$

The above density matrix given in Eq. (26) is obtained from Eq. (8) through replacing $d_{\alpha\beta,\lambda\gamma}$ by $\sqrt[4]{\mu_n} = \sqrt{\mu_n'}$. This density matrix can be reduced to a simplified form when $d \neq 0$ with $\mu_2 = \mu_3$. On the other hand, when $d = 0$ and $\delta \to 0$ one has $\mu_4 = 1$ and $\mu_2 \to \mu_3$, respectively.

The four eigenvalues obtained from $\rho_s\hat{\rho}_s$ with $\mu_2 = \mu_3$ are given by

$$\begin{aligned} \epsilon_1 &= (-1+\sqrt{\mu_4'})^2, \quad \epsilon_2 = (-1+\sqrt{\mu_1'})^2, \\ \epsilon_{3,4} &= \tfrac{1}{2}(2 - 8\mu_3' + 2\sqrt{\mu_4'} + \mu_4' + 2\sqrt{\mu_1'} + \mu_1' \\ &\quad \mp \sqrt{(\sqrt{\mu_4'} - \sqrt{\mu_1'})^2[-16\mu_3' + (2+\sqrt{\mu_4'}+\sqrt{\mu_1'})^2]}) \end{aligned} \tag{27}$$

One can also show that the concurrence, obtained using the above eigenvalue in terms of μ_n, becomes maximum when $\mu_1 \to 0$ while μ_4 and μ_2 are nonzero. This is depicted in Fig. 11(a) where concurrence is plotted as a function of μ_1 and μ_2; concurrence shows a nearly monotonic increase with decreasing μ_1. This justifies the maximization of concurrence that happens for the $d = 0$ case when $\mu_1 \to 0$. However, μ_2 and μ_3 are not always the same for the $d = 0$ case except for the $\delta \to 0$ limit. We consider the simplified situation $\mu_2 = \mu_3$ and $\mu_4 = 1$ to show explicitly that the concurrence indeed maximizes with the $\mu_1 \to 0$ limit. This feature is common when $\mu_4 < 1$ (for the $d \neq 0$ case) and $\mu_2 \neq \mu_3$ (for the $d = 0$ case).

Now we shall examine the second peak observed in C when $\mu_2\mu_3 \to 0$ for any value of d. In order to investigate this

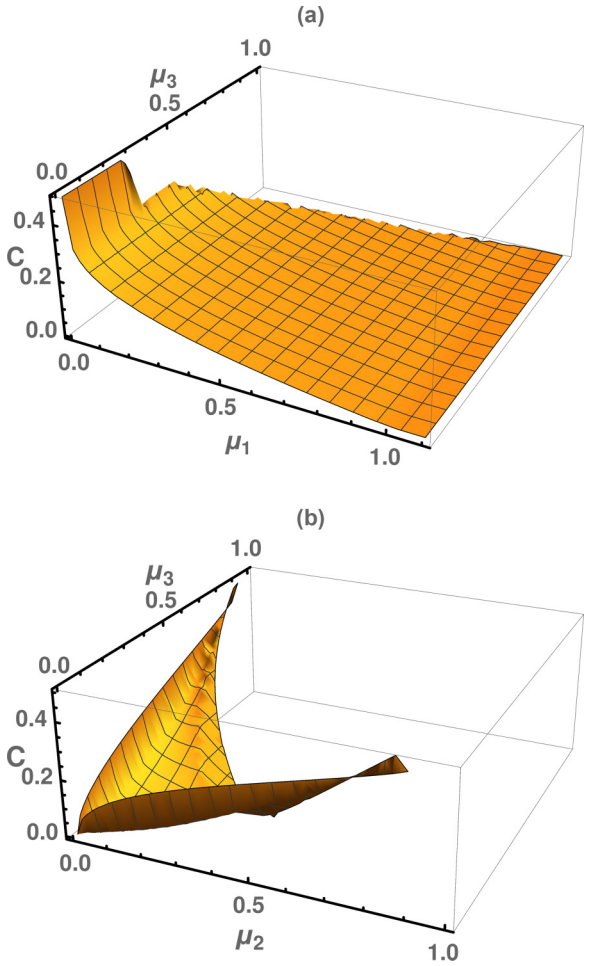

FIG. 11. We plot C obtained from the reduced two qubits density matrix with $\mu_4 = 1$ as a function of μ_1 and μ_2 [with $\mu_2 = \mu_3$ in Eq. (26)] in (a) and as a function of μ_2 and μ_3 (with $\mu_1 = 0$) in (b). Plot (a) indicates that the concurrence, calculated using Eq. (27), becomes maximum for $\mu_1 = 0$. Plot (b) suggests that C, obtained numerically by using Eq. (26), becomes maximum when $\mu_2 \to 0$ with a finite μ_3 and vice versa hence C is maximum in the region $\mu_2\mu_3 \to 0$. The region where C becomes finite is highlighted. The above features hold true for any other value of $\mu_4 \neq 1$.

phenomenon, we have to set $\mu_1 = 0$ in the reduced density matrix presented in Eq. (26). We note that functions involving the product term $\mu_2\mu_3$ appear in the matrix $M = \hat{\rho}_s\rho_s$; hence, the eigenvalues also contain this product, although an analytic closed-form expression of eigenvalues in terms of μ_2, μ_3, and μ_4 cannot be obtained in this case. We present the concurrence, numerically obtained from Eq. (26), in Fig. 11(b) showing that the concurrence is almost a monotonic function of μ_2 (while $\mu_3 \ll 1$) and μ_3 (while $\mu_2 \ll 1$) except near the regions $\mu_2 \leqslant 1$, $\mu_3 \to 0$ and $\mu_3 \leqslant 1$, $\mu_2 \to 0$. We note that the concurrence is finite only in the highlighted region and becomes zero elsewhere. Therefore, it is now clear that C has a secondary maximum when $\mu_2\mu_3 \to 0$ except near the points $\mu_2 = 0$ and $\mu_3 = 0$. This characteristic of concurrence is also seen for the case when $\mu_4 \neq 1$ (for finite d).

Our observation suggests that μ_4 always stays at unity for the $d = 0$ case but concurrence vanishes after the unentanglement time $t_{\rm UE}$. One can therefore infer that concurrence becomes independent of μ_4 and vanishes subsequently when $\mu_1 = \mu_2 = 0$; this can be easily seen by calculating the concurrence from the density matrix (26). Now, for the case $d = 0$, concurrence vanishes immediately after $\sqrt{\mu_3} \to 0$ as shown in Figs. 9(a)–9(c). Under the small δ approximation, one can therefore conclude that $\mu_2 \simeq \mu_3$ is the killing channel which can destroy the concurrence. On the other hand, for $d \neq 0$, it is shown that concurrence vanishes after $\mu_3 \to 0$ instead of $\mu_3^{1/2}$ for the $d = 0$ case. We can say that in the $\delta \to 0$ limit μ_2 or μ_3 is the killing channel for destroying the concurrence. Once $\mu_1 \to 0$, $\mu_2 \to 0$, and $\mu_3 \to 0$ then concurrence becomes independent of the other channel μ_4. This can be seen in the temporal behavior of C for $d = 0$ and $d \neq 0$, where C vanishes even in the presence of a finite μ_4.

We shall now explain the existence of a threshold time $t_{\rm TH}$ [see Figs. 10(a)–10(c)] in the light of above channel analysis. We here connect the behavior observed for μ_n in Figs. 10(a)–10(c) to μ_n' to write the reduced density matrix of the two qubits up to the threshold time $t_{\rm TH}$ given by

$$\rho_s(t) = \frac{1}{4}\begin{bmatrix} 1 & \sqrt{\mu_3'} & \sqrt{\mu_3'} & \mu_3' \\ \sqrt{\mu_3'} & 1 & \mu_3' & \sqrt{\mu_3'} \\ \sqrt{\mu_3'} & \mu_3' & 1 & \sqrt{\mu_3'} \\ \mu_3' & \sqrt{\mu_3'} & \sqrt{\mu_3'} & 1 \end{bmatrix}. \tag{28}$$

This is obtained from (26) by considering the numerically observed behavior of DCs for the $d \neq 0$ case, $\mu_4 = \mu_1$, $\mu_2 = \mu_3$, and $\mu_3^2 = \mu_1$ (i.e., $\mu_4' = \mu_1'$, $\mu_2' = \mu_3'$, and $\mu_3'^2 = \mu_1'$). One can compute the concurrence using the above density matrix (28). All the eigenvalues of $\rho_s\hat{\rho}_s$ are same, i.e., $\epsilon_1 = \epsilon_2 = \epsilon_3 = \epsilon_4 = (-1 + \mu_3')^2$. This yields zero concurrence when $t < t_{TH}$ up to which the above density matrix (28) is valid. After the threshold time, $\mu_4' \neq \mu_1'$, $\mu_3'^2 \neq \mu_1'$ and hence concurrence becomes nonzero even if $\mu_2' = \mu_3'$. This threshold time increases with distance and becomes maximum when the two qubits are separated from each other maximally, i.e., at $d = 50$.

Furthermore, we explore the behavior of four DCs μ_1, μ_2, μ_3, and μ_4 as a function of time by varying the distance between the two qubits. At the outset we note that $v = 2$ and it is independent of the distance between the qubits. Figures 12(a) and 12(d) show that the μ_1 and μ_4 channels are sensitive to d. When the two qubits are at symmetric position (i.e., $d = 50$ for $N = 100$ and PBC), both the channels

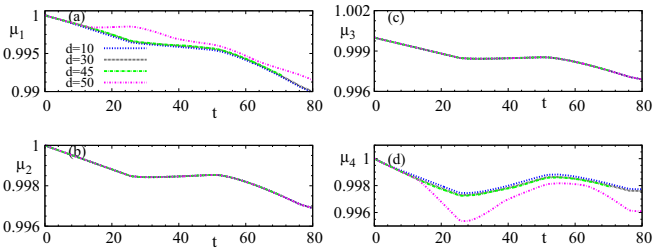

FIG. 12. The temporal behavior of four DCs μ_1 (a), μ_2 (b), μ_3 (c), and μ_4 (d) are plotted as a function of time choosing different values of d. Here, $N = 100$, $\delta = 0.01$, and $\lambda_{i,(f)} = 0.2(0.99)$. The singular and the revival behavior are explained in the text.

exhibit a singular behavior at $t = t_S = N/(4v)$. This singular behavior at t_S does not exist for nonsymmetric situations. It is also to be noted that additionally there is a revival time occurring at $t = t_R = N/(2v)$. The other two channels μ_2 and μ_3 are absolutely insensitive to distance and as a result $t_S = N/(4v)$ is no longer a special time scale for these channels even when $d = 50$ [see Fig. 12(b) and 12(c)]. For the above two channels echo exhibits the singular behavior at $t = t_S = N/(2v)$ which is twice the earlier singular time scale for μ_1 and μ_4. These observations shall now be analyzed in the light of the quasiparticle picture.

When the environmental spin chain is suddenly (and globally) quenched from the FM phase to the QCP, each of the environmental sites emit a pair of quasiparticles moving with opposite momentum in opposite directions. Now, these two quasiparticles meet at $t = t_R = N/(2v)$ after traversing half of the environmental chain and there is a constructive interference causing a partial revival of the initial state (see Fig. 1). The channels μ_1 and μ_4 both involve two distinct Hamiltonians $(H_{\downarrow\downarrow}, H_{\uparrow\uparrow})$ and $(H_{\uparrow\downarrow}, H_{\downarrow\uparrow})$ which are different from each other in terms of the local transverse fields modified through the coupling of the qubits to the two sites; one can think of two extra separate emitters, located at these two sites with distance d away from each other. Now, in the symmetric position $d = N/2$, quasiparticles need to travel only $d/2$ distance for such a revival to happen. Therefore, $t_S = d/(2v) = N/(4v)$ and $t_R = 2t_S$. (Over the former time, two quasiparticles travel $N/4$ while in the latter they traverse a length of $N/2$.) In the case for $d \neq 50$, the singular time scale does not appear, as no constructive interference of two oppositely moving quasiparticles is possible.

What is remarkable is that μ_2 and μ_3 do not exhibit the singular behavior at time $t = t_S$; their dynamical evolution is only governed by the revival time scale t_R [see Figs. 12(b) and 12(d)]. This is due to the fact that one of the underlying Hamiltonians generates an extra pair of quasiparticles than that of the other Hamiltonian involved in μ_2 and μ_3 [i.e., $H_{\downarrow\downarrow}$ is different from $H_{\uparrow\downarrow}$ by a locally modified transverse field at a single site and same for $(H_{\uparrow\uparrow}, H_{\uparrow\downarrow})$]. Therefore, the quasiparticle from this single emitter has to travel a distance $N/2$ to partially recover the initial configuration even if the qubits are separated by a distance $d = N/2$. Therefore, the number of independent emitters, originating from the structure of the two underlying Hamiltonians that govern the dynamics, dictates the time scales of revival and singular behavior. These features are observed in the different channels of echo following a sudden quench.

VI. CONCLUSION

In this paper, we have studied a GCSM where two qubits are locally connected to the environmental transverse Ising spin chain in such a way that the local transverse field of the environment gets modified. Working in the weak-coupling limit, we explore the generation of the entanglement between the above pair of qubits, which are initially completely unentangled, both in equilibrium as well as nonequilibrium situations. In the former situation, the concurrence between them is very small in comparison to the nonequilibrium situation. However, the role of quantum criticality manifests in the behavior of concurrence, as it becomes maximum at the QCP and survives even when d is large; this behavior persists even in the nonequilibrium situation. Additionally, in the latter situation the concurrence remains nonzero for longer time if the quenching is within the same phase. Furthermore, the time at which concurrence exhibits a primary peak is inversely proportional to the coupling strength. Remarkably, we show that there exists a threshold time above which concurrence becomes finite for $d \neq 0$.

Analyzing the behavior of concurrence using different DCs, we show that the number of effectively independent channels is determined by the distance d and the local difference of the transverse field of the two underlying Hamiltonians governing the time evolution of the channels. The interference between a larger number of independent channels may enhance the concurrence. This is a universal observation that holds true for both the equilibrium and nonequilibrium situations. The decoherence is maximum in the channel (μ_1) that involves the maximum difference in the local transverse fields of two Hamiltonians dictating the time evolution; consequently, the short-time decay of the echo is most rapid for this channel in all the situations discussed in the paper. Hence, the time at which this most rapidly decaying DC decays to zero is the primary peak in the concurrence. On the other hand, the product of the intermediate decaying channels $(\mu_2\mu_3)$ is responsible for the secondary peak of the concurrence. Besides these above two common features, there exists a markedly different connection of concurrence with these DCs for a finite separation d. The subsequent temporal decay of concurrence is attributed to the behavior of the killing channel which is an intermediate decaying channel (μ_3); for $d = 0$, the concurrence decays to zero when $\sqrt{\mu_3} \to 0$, while the condition gets modified to $\mu_3 \to 0$ for $d \neq 0$.

Another noteworthy feature exhibited by concurrence in the nonequilibrium case is that it acquires a finite value only above the threshold time when the two qubits are separated from each other by a finite distance. We analyze the existence of a finite threshold time using the channel analysis. Comparing the behavior of the concurrence in the nonequilibrium case with the DP obtained from the reduced single qubit density matrix, we explain the interesting observation that the dephasing rate is always lower than the unentanglement rate. This is a consequence of the fact that DCs appear additively in DP and additionally, the most rapidly DC is absent in the 2×2 reduced density matrix. Finally, we resort to the quasiparticle picture to characterize the temporal evolution of different channels, following a critical quench, with different values of the distance between the qubits as a function of time. We explain the singular and revival behavior of different channels analyzing the interference of quasiparticles. Remarkably, the singular behavior in the evolution shows up only for the maximally and minimally decaying channel denoted by μ_1 and μ_4, respectively.

ACKNOWLEDGMENTS

T.N. and A.D. thank U. Divakaran for her valuable suggestions and numerical help. A.D. acknowledges SERB, DST for financial support.

[1] A. Einstein, B. Podolsky, and N. Rosen, Phys. Rev. **47**, 777 (1935).

[2] R. F. Werner, Phys. Rev. A **40**, 4277 (1989).

[3] C. H. Bennett, D. P. DiVincenzo, J. A. Smolin, and W. K. Wootters, Phys. Rev. A **54**, 3824 (1996).

[4] M. A. Nielsen and I. L. Chuang, *Quantum Computation and Quantum Information* (Cambridge University Press, Cambridge, UK, 2000).

[5] V. Vedral, *Introduction to Quantum Information Science* (Oxford University Press, Oxford, UK, 2007).

[6] Sei Suzuki, Jun-ichi Inoue, and Bikas K. Chakrabarti, *Quantum Ising Phases and Transitions in Transverse Ising Models*, Lecture Notes in Physics 862 (Springer, Heidelberg, 2013).

[7] S. Sachdev, *Quantum Phase Transitions* (Cambridge University Press, Cambridge, UK, 1999).

[8] A. Polkovnikov, K. Sengupta, A. Silva, and M. Vengalattore, Rev. Mod. Phys. **83**, 863 (2011).

[9] A. Dutta, G. Aeppli, B. K. Chakrabarti, U. Divakaran, T. Rosenbaum, and D. Sen, *Quantum Phase Transitions in Transverse Field Spin Models: From Statistical Physics to Quantum Information* (Cambridge University Press, Cambridge, UK, 2015).

[10] A. Osterloh, L. Amico, G. Falci, and R. Fazio, Nature (London) **416**, 608 (2002).

[11] T. J. Osborne and M. A. Nielsen, Phys. Rev. A **66**, 032110 (2002).

[12] G. Vidal, J. I. Latorre, E. Rico, and A. Kitaev, Phys. Rev. Lett. **90**, 227902 (2003).

[13] L. A. Wu, M. S. Sarandy, and D. A. Lidar, Phys. Rev. Lett. **93**, 250404 (2004).

[14] Y. Chen, P. Zanardi, Z. D. Wang, and F. C. Zhang, New J. Phys. **8**, 97 (2006).

[15] S. J. Gu, S. S. Deng, Y. Q. Li, and H. Q. Lin, Phys. Rev. Lett. **93**, 086402 (2004).

[16] L. Amico, R. Fazio, A. Osterloh, and V. Vedral, Rev. Mod. Phys. **80**, 517 (2008).

[17] W. K. Wootters, Quantum Inf. Comp. **1**, 27 (2001).

[18] M. Horodecki, Quantum Inf. Comp. **1**, 3 (2001).

[19] R. Horodecki, P. Horodecki, M. Horodecki, and K. Horodecki, Rev. Mod. Phys. **81**, 865 (2009).

[20] H. Ollivier and W. H. Zurek, Phys. Rev. Lett. **88**, 017901 (2001); W. H. Zurek, Rev. Mod. Phys. **75**, 715 (2003).

[21] S. Luo, Phys. Rev. A **77**, 042303 (2008).

[22] M. S. Sarandy, Phys. Rev. A **80**, 022108 (2009).

[23] P. Calabrese and J. Cardy, J. Stat. Mech.: Theor. Exp. (2005) P04010; (2007) P06008; L. Cincio, J. Dziarmaga, M. M. Rams, and W. H. Zurek, Phys. Rev. A **75**, 052321 (2007).

[24] E. Joos, H. D. Zeh, C. Keifer, D. Giulliani, J. Kupsch, and I.-O. Stamatescu, *Decoherence and Appearance of a Classical World in a Quantum Theory* (Springer, Berlin, 2003).

[25] M. B. Plenio, S. F. Huelga, A. Beige, and P. L. Knight, Phys. Rev. A **59**, 2468 (1999); S. Bose, P. L. Knight, M. B. Plenio, and V. Vedral, Phys. Rev. Lett. **83**, 5158 (1999); P. Horodecki, Phys. Rev. A **63**, 022108 (2001); X. X. Yi, C. S. Yu, L. Zhou, and H. S. Song, *ibid.* **68**, 052304 (2003); S. Shresta, C. Anastopoulos, A. Dragulescu, and B. L. Hu, *ibid.* **71**, 022109 (2005); N. Wu, A. Nanduri, and H. Rabitz, *ibid.* **89**, 062105 (2014).

[26] L. Viola and S. Lloyd, Phys. Rev. A **58**, 2733 (1998).

[27] D. Rossini, T. Calarco, V. Giovannetti, S. Montangero, and R. Fazio, Phys. Rev. A **75**, 032333 (2007); D. Rossini, P. Facchi, R. Fazio, G. Florio, D. A. Lidar, S. Pascazio, F. Plastina, and P. Zanardi, *ibid.* **77**, 052112 (2008); T. Fogarty, E. Kajari, B. G. Taketani, A. Wolf, Th. Busch, and G. Morigi, *ibid.* **87**, 050304 (2013); B. G. Taketani, T. Fogarty, E. Kajari, Th. Busch and G. Morigi, *ibid.* **90**, 012312 (2014).

[28] F. M. Cucchietti, J. P. Paz, and W. H. Zurek, Phys. Rev. A **72**, 052113 (2005); F. M. Cucchietti, S. Fernandez-Vidal, and J. P. Paz, *ibid.* **75**, 032337 (2007).

[29] H. T. Quan, Z. Song, X. F. Liu, P. Zanardi, and C. P. Sun, Phys. Rev. Lett. **96**, 140604 (2006).

[30] S. Sharma, V. Mukherjee, and A. Dutta, Eur. Phys. J. B **85**, 143 (2012).

[31] B. Damski, H. T. Quan, and W. H. Zurek, Phys. Rev. A **83**, 062104 (2011).

[32] T. Nag, A. Dutta, and A. Patra, Int. J. Mod. Phys. B **27**, 1345036 (2013).

[33] T. Nag, U. Divakaran, and A. Dutta, Phys. Rev. B **86**, 020401(R) (2012).

[34] S. Roy, T. Nag, and A. Dutta, Eur. Phys. J. B **86**, 204 (2013).

[35] A. A. Patel, S. Sharma, and A. Dutta, Eur. Phys. J. B **86**, 367 (2013).

[36] V. Mukherjee, S. Sharma, and A. Dutta, Phys. Rev. B **86**, 020301(R) (2012).

[37] S. Sharma, A. Russomanno, G. E. Santoro, and A. Dutta, Europhys. Lett. **106**, 67003 (2014).

[38] S. Suzuki, T. Nag, and A. Dutta, Phys. Rev. A **93**, 012112 (2016).

[39] T. Nag, Phys. Rev. E **93**, 062119 (2016).

[40] M. Heyl, A. Polkovnikov, and S. Kehrein, Phys. Rev. Lett. **110**, 135704 (2013).

[41] S. Sharma, S. Suzuki, and A. Dutta, Phys. Rev. B **92**, 104306 (2015).

[42] K. Sengupta and D. Sen, Phys. Rev. A **80**, 032304 (2009).

[43] T. Nag, A. Patra, and A. Dutta, J. Stat. Mech. (2011) P08026.

[44] W. H. Zurek, U. Dorner, and P. Zoller, Phys. Rev. Lett. **95**, 105701 (2005).

[45] A. Polkovnikov, Phys. Rev. B **72**, 161201 (2005).

[46] Z. G. Yuan, P. Zhang, and S.-S. Li, Phys. Rev. A **76**, 042118 (2007).

[47] Z. Sun, X. Wang, and C. P. Sun, Phys. Rev. A **75**, 062312 (2007).

[48] B.-Q. Liu, B. Shao, and J. Zou, Phys. Rev. A **82**, 062119 (2010).

[49] X. X. Yi, H. T. Cui, and L. C. Wang, Phys. Rev. A **74**, 054102 (2006).

[50] Q. Ai, T. Shi, G. Long, and C. P. Sun, Phys. Rev. A **78**, 022327 (2008).

[51] M. Greiner, O. Mandel, T. Esslinger, T. W. Hänsch, and I. Bloch, Nature (London) **415**, 39 (2002).

[52] L. M. Duan, E. Demler, and M. D. Lukin, Phys. Rev. Lett. **91**, 090402 (2003); D. Porras and J. I. Cirac, *ibid.* **92**, 207901 (2004); J. K. Pachos and M. B. Plenio, *ibid.* **93**, 056402 (2004).

[53] J. Zhang, F. M. Cucchietti, C. M. Chandrashekar, M. Laforest, C. A. Ryan, M. Ditty, A. Hubbard, J. K. Gamble, and R. Laflamme, Phys. Rev. A **79**, 012305 (2009).

[54] C. Cormick and J. P. Paz, Phys. Rev. A **78**, 012357 (2008).

[55] P. Wendenbaum, B. G. Taketani, and D. Karevski, Phys. Rev. A **90**, 022125 (2014).

[56] M. J. Hartmann, M. E. Reuter, and M. B. Plenio, New J. Phys. **8**, 94 (2006).
[57] E. Lieb, T. Schultz, and D. Mattis, Ann. Phys. (NY) **16**, 37004 (1961).
[58] P. Pfeuty, Ann. Phys. (NY) **57**, 79 (1970).
[59] M. Keyl and D.-M. Schlingemann, J. Math. Phys. **51**, 023522 (2010).
[60] T. Yu and J. H. Eberly, Phys. Rev. B **68**, 165322 (2003); K. Ann and G. Jaeger, *ibid.* **75**, 115307 (2007).